NANO LETTERS

pubs.acs.org/NanoLett

Light Trapping in Silicon Nanowire Solar Cells

Erik Garnett and Peidong Yang*

Department of Chemistry, University of California, Berkeley, California 94720

ABSTRACT Thin-film structures can reduce the cost of solar power by using inexpensive substrates and a lower quantity and quality of semiconductor material. However, the resulting short optical path length and minority carrier diffusion length necessitates either a high absorption coefficient or excellent light trapping. Semiconducting nanowire arrays have already been shown to have low reflective losses compared to planar semiconductors, but their light-trapping properties have not been measured. Using optical transmission and photocurrent measurements on thin silicon films, we demonstrate that ordered arrays of silicon nanowires increase the path length of incident solar radiation by up to a factor of 73. This extraordinary light-trapping path length enhancement factor is above the randomized scattering (Lambertian) limit ($2n^2 \sim 25$ without a back reflector) and is superior to other light-trapping methods. By changing the silicon film thickness and nanowire length, we show that there is a competition between improved absorption and increased surface recombination; for nanowire arrays fabricated from 8 μm thick silicon films, the enhanced absorption can dominate over surface recombination, even without any surface passivation. These nanowire devices give efficiencies above 5%, with short-circuit photocurrents higher than planar control samples.

KEYWORDS Silicon, nanowires, solar cell, light trapping

Over the last 50 years, commercial silicon photovoltaics have been developed to convert sunlight into electricity at efficiencies around 20% and provide the most feasible carbon-neutral route to displacing terawatts (TW) of nonrenewable power consumed worldwide.[1] However, large-scale implementation is currently not economically feasible because of the high cost as compared to traditional power sources. One of the primary costs for silicon photovoltaic cells is the starting silicon wafer, which requires extensive purification to maintain reasonable performance.[2−4] Therefore, reducing the required silicon's quality and quantity will help drive large-scale implementation of silicon photovoltaics. Using solar cells with nanostructured radial p−n junctions may solve both of these problems simultaneously by orthogonalizing the direction of light absorption and charge separation while allowing for improved light scattering and trapping.[5] Previously, the highest efficiency silicon nanowire radial p−n junction solar cells required vapor−liquid−solid (VLS) nanowire growth from gold colloid particles, in situ thin-film deposition, multiple electron-beam lithography (EBL) steps and carefully timed silicon etching to contact the p- and n-type layers selectively.[6] Even with this complicated processing, the resulting solar cells showed very low efficiency unless an intrinsic silicon thin-film layer was inserted in between the p- and n-type layers. With the p−i−n structure, the single nanowire solar cells still showed a low open circuit voltage (V_{oc}) of 0.26 V. A moderate overall efficiency of 2.3−3.4% was possible because of an extraordinarily high short-circuit current density (J_{sc}), which was attributed to strongly enhanced absorption in the thin-film shell because of its nanocrystalline nature.

In contrast, our approach has focused on large-area, scalable, and simple fabrication methods for making solar cells from arrays of silicon nanowires with radial p−n junctions. We have already demonstrated a room temperature aqueous etching method followed by low-temperature thin-film deposition and a rapid thermal annealing crystallization step to make wafer-scale radial p−n junction solar cells, but the efficiency was only about 0.5% primarily because of a low V_{oc} and poor fill factor (FF).[7] In this report, our improved process maintains the advantages of our previous work but also dramatically reduces surface roughness and improves control over the nanowire diameter and density. This new method leads to greatly enhanced V_{oc}, FF, and J_{sc} values, ultimately yielding 10 times higher efficiencies using thin silicon absorber films. We also quantitatively measure strong light trapping effects, with path length enhancement factors up to 73, which help improve J_{sc} over planar controls, despite the increased surface and junction recombination that is associated with the nanowire geometry.

The fabrication method consists of four simple steps illustrated in Figure 1: silica bead synthesis,[8] dip coating to form a self-assembled monolayer of beads on the silicon surface, deep reactive ion etching to form the nanowire array,[9] and diffusion to form the p−n junction. Figure 2a shows scanning electron microscopy (SEM) images of silica bead monolayers assembled on silicon via dip coating. The excellent packing shown in the SEM images extends over large areas, up to 10 cm^2, limited now by the size of the dip-coating cell. The monolayer films of silica beads were used as a mask for deep reactive ion etching (DRIE) with SF_6 to form uniform periodic nanowire arrays (Figure 2b,c). The nanowire pitch and diameter are controlled by the silica

* To whom correspondence should be addressed, p_yang@berkeley.edu.
Received for review: 01/17/2010
Published on Web: 01/28/2010

DOI: 10.1021/nl100161z | *Nano Lett.* **2010,** *10,* 1082–1087

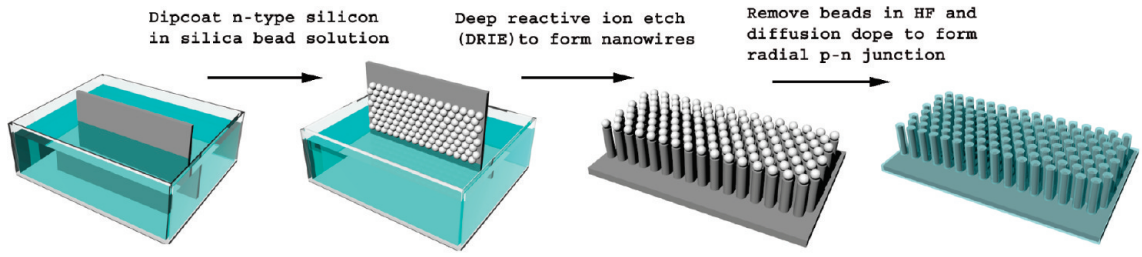

FIGURE 1. Ordered silicon nanowire array fabrication scheme. The fabrication consisted of three major steps depicted above: dip coating an n-type silicon wafer in an aqueous suspension of silica beads to get a close-packed monolayer; deep reactive ion etching (DRIE) using the beads as an etch mask to form nanowires; bead removal in HF and boron diffusion to form the radial p−n junction. Standard photolithography and metal sputtering were used for the top finger grid while metal evaporation provided the back contact (not shown).

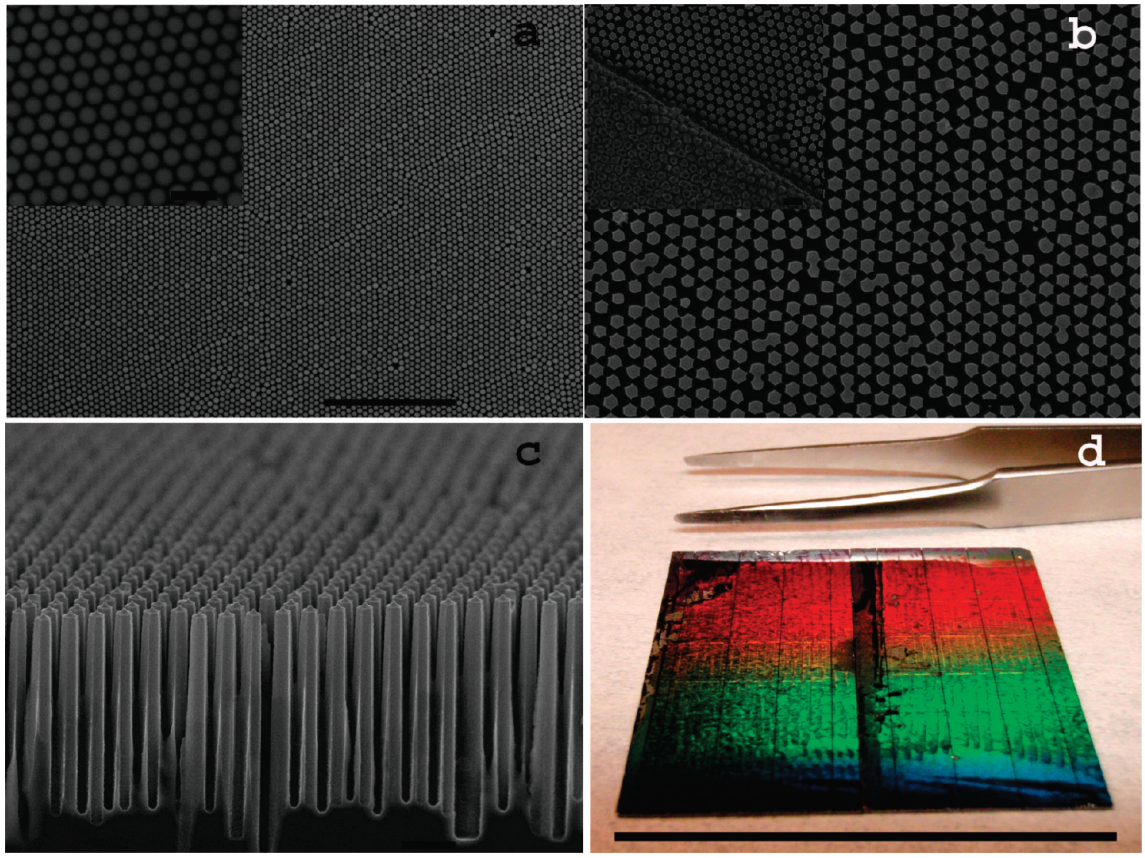

FIGURE 2. Solar cell fabrication and structure. (a) Scanning electron micrograph (SEM) of a close-packed monolayer of silica beads assembled on a silicon wafer using dip coating. Scale bars are 10 and 1 μm for the main picture and inset, respectively. (b) Plan view SEM of a completed ordered silicon nanowire radial p−n junction array solar cell made by bead assembly and deep reactive ion etching. The inset shows the edge of a top contact finger, demonstrating that the metal completely fills in between the nanowires. Scale bars are 1 μm. (c) Tilted cross-sectional SEM of the solar cell in panel b. Scale bar is 1 μm. (d) Tilted optical image of 36 silicon nanowire radial p−n junction solar cell arrays from (a−c). The color dispersion demonstrates the excellent periodicity present over the entire substrate. Scale bar is 4 cm.

bead diameter, while the length is determined by the DRIE time. Because of partial etching of the silica bead mask, the final nanowire diameter is always smaller than the starting bead diameter and is coupled to the etch time; for our standard 8 min etch the diameter was 390 nm when using 530 nm beads and the length was about 5 μm. After DRIE, the mask was removed with hydrofluoric acid and the radial p−n junction was formed via boron diffusion into the starting n-type silicon wafer. The junction depth was calculated to be about 160 nm. Our previous work has shown that diffusion in silicon nanowires gives radial doping profiles that match well with those calculated using standard diffusion equations.[10] Photolithography and aluminum/palladium sputtering led to a top contact grid with metal filling completely between the nanowires, which allowed for probing without breaking any nanowires (Figure 2b, inset).

Figure 2d shows an optical image of the completed devices on a 16 cm^2 substrate; the iridescent color gradient is caused by white light interacting with the periodic nanowire array at different angles, demonstrating the excellent

DOI: 10.1021/nl100161z | Nano Lett. 2010, 10, 1082–1087

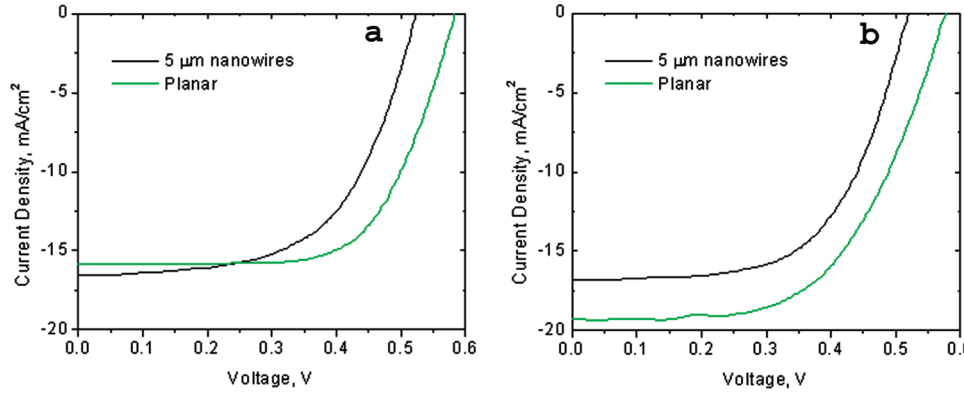

FIGURE 3. Solar cell output characteristics. (a) 5 μm nanowire and planar control solar cells fabricated from an 8 μm thin silicon absorber. (b) The same structures as in panel a, but using a 20 μm thin silicon absorber.

uniformity over large areas that can be achieved with this technique. Each of the 36 solar cells located on the same substrate is electrically isolated from the others by mechanical sawing. As substrates for the dip coating and subsequent solar cell fabrication, we used very highly doped n-type silicon wafers with two different doping levels, each with a thin, lightly doped epitaxial layer on top. Since the minority carrier diffusion length depends on the doping concentration,[11] these wafers allowed us to mimic the photovoltaic response of very thin silicon solar cells—8 and 20 μm in our case—while avoiding complications associated with handling such thin silicon wafers or depositing and contacting multicrystalline silicon on a low-cost substrate. This simple method for varying the silicon solar cell thickness also allows for quantitative measurements of the nanowire array's light trapping efficiency, as will be discussed later. Even though low-cost substrates were not used in this proof-of-concept study, the fabrication procedure demonstrated here should be transferable to multicrystalline silicon (or even other semiconductor) thin films deposited on low-cost substrates, such as glass, aluminum, or metallurgical grade silicon.[12]

Figure 3 shows the output characteristics of 5 μm nanowire and planar control solar cells under AM1.5G illumination for two different silicon absorber thicknesses. The average V_{oc} and FF values of 0.519 ± 0.003 V and 0.607 ± 0.005 for the 20 μm absorbing layer and 0.525 ± 0.002 V and 0.559 ± 0.02 for the 8 μm absorbing layer are higher than previously reported values for silicon nanowire core−shell p−n junction photovoltaics.[6,7] The average J_{sc} values of 16.82 ± 0.50 and 16.45 ± 0.19 mA/cm^2 give an overall efficiency of 5.30 ± 0.19% and 4.83 ± 0.19% for the 20 and 8 μm cells, respectively. The 2% increase in J_{sc} for the thicker nanowire cell is much smaller than the expected 20% increase calculated from the absorption for a single pass through the different silicon layer thicknesses and the 22% increase shown in the planar control samples. This suggests the periodic vertical nanowire arrays provide a strong light trapping effect, which will be discussed in detail later.

The 4.83% average efficiency for the 8 μm absorber silicon nanowire array solar cells is about 20% higher than results on 8 μm thick silicon ribbon solar cells, while the 20 μm absorber silicon nanowire cell average efficiency of 5.30% is about 35% lower than equivalent ribbon cells,[13] demonstrating that the nanowire geometry provides superior light trapping but also dramatically increases surface and junction recombination. For very thin absorbing layers the light-trapping effects dominate, while for thicker cells that already absorb a large fraction of the incident light, the recombination effect is more important. Indeed, planar controls fabricated in parallel on the 8 μm silicon absorbing layer wafers showed a 4% lower J_{sc} versus the nanowire cells, but planar controls made using the 20 μm silicon absorbing layers had a 14% higher J_{sc} than nanowire cells. Previous reports advocating silicon nanowire array solar cells have shown they exhibit excellent antireflection properties but have not considered additional light-trapping effects.[14−18] In order to explore the optical trapping advantages and recombination disadvantages of nanowire arrays, we have fabricated arrays with the same periodicity but with different lengths on several different silicon absorbing layer thicknesses and measured their optical transmission spectra and photovoltaic characteristics.

Figure 4 shows tilted cross-sectional SEM images and corresponding transmission measurements of thin silicon membranes patterned with nanowire arrays of two different lengths. The membranes were prepared by etching windows in the handle of silicon on insulator (SOI) wafers through a silicon nitride mask using KOH. The buried oxide acts as an etch stop, giving windows with only the thin silicon device layer remaining. The SOI device layer was chosen to have a similar thickness to the 8 μm thin silicon absorber solar cells to allow for direct comparison. These wafers with thin silicon windows were used for nanowire fabrication following the bead assembly and etching procedure discussed previously. The standard 8 min etch yields nanowires that are about 5 μm long so that most of the membrane has a nanowire structure, while the 4 min etch leads to about 2 μm short

DOI: 10.1021/nl100161z | *Nano Lett.* **2010,** *10,* 1082–1087

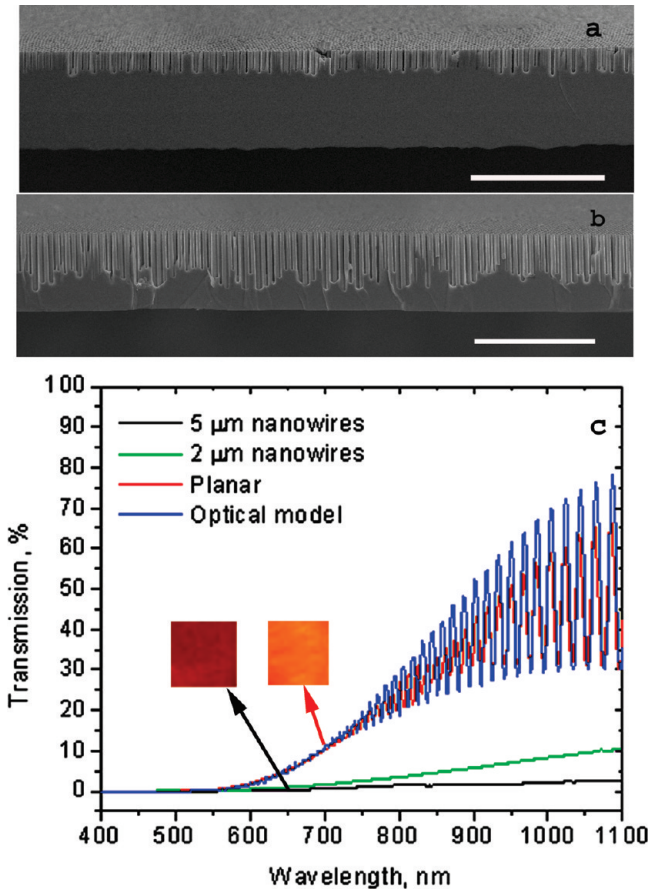

FIGURE 4. Optical transmission measurements on thin silicon windows with and without nanowires. Tilted cross-sectional SEM images of (a) 2 μm nanowire arrays and (b) 5 μm nanowire arrays on 7.5 μm thick silicon windows. Both scale bars are 10 μm. (c) Transmission spectra of thin silicon window structures before (red) and after etching to form 2 μm (green) and 5 μm (black) nanowires. The spectra from an optical model for a 7.5 μm thin silicon window is in blue and matches very well with the planar control measurement. The insets are backlit color images of the membranes before and after etching. Clearly there is a large intensity reduction and red shift in the transmitted light after the nanowires are formed, suggesting strong light trapping.

nanowires that penetrate into only the top 25% of the membrane (Figure 4). Optical measurements performed on these membranes before and after nanowire fabrication show that the transmission over the entire spectral range from 600 to 1100 nm is reduced by factors of 2.9−7.8 and 12−29 for the 2 and 5 μm nanowires, respectively (Figure 4c). The planar control shows strong interference patterns and is in excellent agreement with an optical model for a 7.5 μm thin silicon membrane (details in Supporting Information). The insets in Figure 4c show backlit color images of the windows with and without nanowires; clearly the nanowire arrays reduce the intensity and red shift the frequency of the transmitted light, as expected for a strong light-trapping effect. It is possible that the nanowires simply act as very effective scattering centers and that some (or even a majority) of the light is coupled out of the membrane at some angle so that it does not strike the detector. One way to confirm that the periodic vertical nanowire array truly traps light and leads to increased absorption is to monitor the J_{sc} as a function of nanowire length for thin silicon solar cells that can benefit significantly from an increased effective path length.

Figure 5a shows the photovoltaic characteristics for 8 μm cells fabricated with various nanowire lengths, leading to different roughness factors. The roughness factor (RF) is defined as the actual surface area of the structure divided by the geometric area (e.g., RF of a planar cell is 1). The V_{oc}, FF, and J_{sc} trends show that the increased surface and junction areas lead to both enhanced recombination (lower V_{oc}, FF) and improved light trapping (higher J_{sc}). It also appears that the light-trapping effect dominates over the surface and junction recombination effect for this silicon absorber thickness, as the J_{sc} continues to increase with higher RF. The correlation between J_{sc} and RF is especially striking when considering that by increasing the nanowire length, the amount of silicon left to absorb light is decreasing significantly and a much higher fraction of the remaining silicon is in close proximity to the surface and p−n junction, increasing the probability of carrier recombination. In order to correct for the reduced volume, the J_{sc} was normalized by the fraction of light that should be absorbed as compared to the planar control (Figure 5a, normalized J_{sc}).

The RF-dependent recombination effect was removed by comparing the J_{sc} of silicon nanowire array solar cells with the same RF, and thus the same surface and junction recombination characteristics, but with different absorbing layer thicknesses. In this way, we can quantitatively extract light-trapping path length enhancement factors (EF) for different nanowire geometries (full derivation in Supporting Information). Figure 5b shows the minimum and maximum EF as a function of RF plotted on a semilog scale compared to the normalized J_{sc} from Figure 5a on a linear scale. The strong correlation further supports the light-trapping effect, as the absorption (and thus J_{sc}) should increase logarithmically with the path length. The transmission measurements in Figure 4c can also be used to calculate an EF as a function of RF. In this case, there is uncertainty as to how much of the reduced transmission comes from absorption versus how much is from scattered light that does not couple into the cell and is ultimately lost. From the photocurrent data, the light-trapping efficiency clearly increases with RF, so we would expect that the fraction of scattered light that leads to absorption would also increase with RF. If we assume this coupling efficiency is proportional to the logarithm of RF and set a coupling efficiency of 95% (after reflection losses) for the longest nanowires, then we get EF of 2.0 and 62 for the shortest and longest nanowires, respectively, in excellent agreement with the maximum EF from the J_{sc} data that varied between 1.7 and 73 (Figure 5). If instead we assume an 85% coupling efficiency, we get EF of 1.2 and 8.3 for the shortest and longest nanowires, respectively, close to the minimum EF from the J_{sc} data of 0.96 and 11. This demon-

DOI: 10.1021/nl100161z | *Nano Lett.* **2010,** *10,* 1082–1087

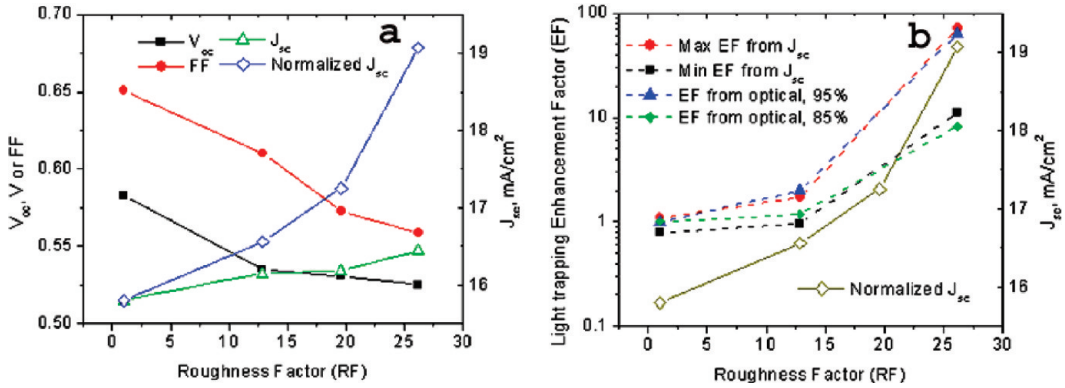

FIGURE 5. Photovoltaic response and light-trapping effect as a function of roughness factor. (a) The V_{oc}, FF, and J_{sc} of periodic silicon nanowire array solar cells fabricated from an 8 μm thick silicon absorber with three different roughness factors (RF) compared to a planar control (RF = 1). The normalized J_{sc} is determined by dividing the nanowire J_{sc} by the fraction of light that should be absorbed compared to the planar control, considering the loss in volume for the nanowire cells. The increasing J_{sc} with higher RF suggests that the light trapping effect induced by ordered nanowire arrays is sufficient to overcome the increased surface and junction recombination that comes with longer nanowires. (b) Light-trapping path length enhancement factor (EF) vs RF on a semilog scale derived by comparing the J_{sc} from ordered silicon nanowire arrays with the same RF but different absorber thicknesses (red and black) and from the optical transmission measurements in Figure 3c, assuming 95% (blue) or 85% (green) of the reduced transmission ultimately leads to absorption. The normalized J_{sc} (brown) is also shown on a linear scale for comparison. The strong correlation further supports the light-trapping effect since absorption (and ultimately photocurrent) scales with the logarithm of the path length.

strates that there is very good coupling and an extraordinary light-trapping effect, exceeding the theoretical maximum of $2n^2$ (~25 for Si), where n is the refractive index, for ideal randomizing (Lambertian) schemes without a back reflector.[19−21] It is important to recognize that these extraordinary EF results include the entire AM1.5G spectrum (above the silicon band gap), suggesting that the EF at wavelengths near the band gap must be much higher. Indeed, using the transmission measurements as described above gives EF of 156−210 at 1050 nm for 85−95% coupling efficiency.

Calculations have shown that certain periodic structures are capable of exceeding the Lambertian EF limit,[20,22−24] including orthogonal grooves on opposite sides of a silicon slab (EF 50−70)[20] and photonic crystals coupled to a planar absorber (EF >100 for certain wavelength ranges).[22] One study predicted a maximum EF for solar cells coupled to photonic crystals consisting of silicon pillars with a period of approximately 500 nm and a diameter of 390 nm, nearly identical to what we have produced here (though they examined a square lattice and our structures have a hexagonal lattice).[22] However, without comparing arrays of different periods and even random spacing, we cannot conclusively say that our cells show a photonic crystal enhancement effect. Despite the incredible light trapping, these nanowire structures still do not exceed the overall efficiency of planar cells, at least for silicon layers above 8 μm in thickness, due to enhanced surface and junction recombination. We did not perform any surface passivation, which is known to be important in high-performance planar solar cells and should be even more critical for these devices. Proper surface treatments and improved nanowire array geometries that allow for lower roughness factors without sacrificing light trapping will be critical to achieve high efficiency ultrathin silicon solar cells.

In conclusion, we have demonstrated a simple and scalable method to fabricate large-area silicon nanowire radial p−n junction photovoltaics. It requires dip coating a silicon substrate to self-assemble silica spheres, DRIE to form nanowires and diffusion to form the p−n junction. We achieved efficiencies of between 5 and 6% for these ordered vertical silicon nanowire array solar cells on 20 and 8 μm silicon absorber layers with different roughness factors. By comparing the photovoltaic output characteristics of these different cells, we show that longer nanowires lead to both increased recombination and higher absorption, with the light-trapping effect dominating for 8 μm thin silicon absorbing layers. We quantitatively measure a maximum light trapping path length enhancement factor over the entire AM1.5G spectrum between 1.7 and 73, depending on the nanowire geometry, which agrees well with enhancement factors between 2 and 62 extracted from optical transmission measurements. This light-trapping ability is above the theoretical limit for a randomizing scheme, indicating that there may be photonic crystal enhancement effects present in our devices. This ordered vertical nanowire array geometry represents a viable path toward high-efficiency, low-cost thin-film solar cells by providing a way to reduce both the quantity and quality of the required semiconductor.

Acknowledgment. We thank Akram Boukai and Sarah Brittman for reviewing the manuscript. NSF-COINS provided funding for this project. P.Y. would like to thank NSF for the Waterman Award.

Supporting Information Available. Methods, enhancement factor, and planar transmission model calculation details. This material is available free of charge via the Internet at http://pubs.acs.org.

DOI: 10.1021/nl100161z | *Nano Lett.* **2010,** *10,* 1082–1087

REFERENCES AND NOTES

(1) Lewis, N. S.; Nocera, D. G. *Proc. Natl. Acad. Sci. U.S.A.* **2007**, *104*, 20142–20152.
(2) Fawer-Wasswer, M. Solar energy—sunny days ahead? Current status and outlook for photovoltaics and solar thermal power. *Sarasin Sustainable Investment Report*, **2004**.
(3) Green, M. A. *Sol. Energy* **2004**, *76*, 3–8.
(4) Alsema, E. A. *Prog. Photovoltaics* **2000**, *8*, 17–25.
(5) Kayes, B. M.; Atwater, H. A.; Lewis, N. S. *J. Appl. Phys.* **2005**, *97*, 114302.
(6) Tian, B. Z.; et al. *Nature* **2007**, *449*, 885–888.
(7) Garnett, E. C.; Yang, P. *J. Am. Chem. Soc.* **2008**, *130*, 9224–9225.
(8) Bogush, G. H.; Tracy, M. A.; Zukoski, C. F. *J. Non-Cryst. Solids* **1988**, *104*, 95–106.
(9) Hsu, C.; Connor, S. T.; Tang, M. X.; Cui, Y. *Appl. Phys. Lett.* **2008**, *93*, 133109.
(10) Garnett, E. C.; et al. *Nat. Nanotechnol.* **2009**, *4*, 311–314.
(11) Delalamo, J. A.; Swanson, R. M. *Solid-State Electron.* **1987**, *30*, 1127–1136.
(12) Green, M. A.; et al. *Sol. Energy* **2004**, *77*, 857–863.
(13) Yoon, J.; et al. *Nat. Mater.* **2008**, *7*, 907–915.
(14) Peng, K. Q.; et al. *Small* **2005**, *1*, 1062–1067.
(15) Fang, H.; Li, X. D.; Song, S.; Xu, Y.; Zhu, J. *Nanotechnology* **2008**, *19*, 255703.
(16) Zhu, J.; et al. *Nano Lett.* **2009**, *9*, 279–282.
(17) Hu, L.; Chen, G. *Nano Lett.* **2007**, *7*, 3249–3252.
(18) Muskens, O. L.; Rivas, J. G.; Algra, R. E.; Bakkers, E. P. A. M.; Lagendijk, A. *Nano Lett.* **2008**, *8*, 2638–2642.
(19) Yablonovitch, E.; Cody, G. D. *IEEE Trans. Electron Devices* **1982**, *29*, 300–305.
(20) Campbell, P.; Green, M. A. *J. Appl. Phys.* **1987**, *62*, 243–249.
(21) Green, M. A. Silicon Solar Cells: Advanced Principles & Practice; University of New South Wales, 1995.
(22) Zhou, D. Y.; Biswas, R. *J. Appl. Phys.* **2008**, *103*, No. 093102.
(23) Chutinan, A.; Kherani, N. P.; Zukotynski, S. *Opt. Express* **2009**, *17*, 8871–8878.
(24) Bermel, P.; Luo, C.; Zeng, L.; Kimerling, L. C.; Joannopoulos, J. D. *Opt. Express* **2007**, *15*, 16986–17000.

DOI: 10.1021/nl100161z | *Nano Lett.* **2010,** *10,* 1082–-1087

Supporting Information

Light trapping in silicon nanowire solar cells

Erik Garnett and Peidong Yang
Department of Chemistry, University of California, Berkeley, CA 94720

Methods

Synthesis of silica spheres

10 mL concentrated ammonium hydroxide, 7 mL water and 31 mL ethanol were added to a round bottom flask and stirred at 800 RPM. 3 mL tetraethylorthosilicate (TEOS) were injected and the reaction proceeded for 8 hours at room temperature giving 400 nm diameter beads. A secondary injection consisting of 3 mL TEOS and 0.5 mL water increased the size of the beads to 530 nm without creating more nucleates. After 4 hours, the beads were centrifuged and washed four times with water before being suspended in 7.5 mL of water. This solution was used for dipcoating.

Silicon wafer preparation for dipcoating

Silicon wafers were n-type and consisted of a low resistivity substrate with a thin, high resistivity epixtaxial layer. The 20 and 8 μm absorbing layer wafers had bulk wafers with resistivities of 0.01 and 0.001 Ω•cm, respectively with 5 and 7.5 μm epitaxial layers with resistivites of 10 and 0.8 Ω•cm, respectively. The total absorbing layer thicknesses were estimated by adding the minority carrier diffusion lengths in the highly-doped bulk wafers of 15 μm and 0.5 μm taken from literature to the lightly-doped epitaxial layer thicknesses. The thickness ratio was consistent with photocurrent measurements on planar control solar cells fabricated in parallel. The wafers were

sonicated for several minutes in acetone and isopropanol, cleaned with oxygen plasma for 5 minutes, boiled in piranha (concentrated H_2SO_4:30% H_2O_2 1:3) for at least 2 hours, rinsed with water and blown dry with nitrogen. This treatment ensured a clean and hydrophilic surface and was important to achieve uniform, large-area close-packed monolayer films of silica beads.

Dipcoating

The dipcoating assembly contained a syringe pump connected to a thick wire terminating in a clip for the silicon wafer, a glass cuvette 50 mm long with a 2 mm wide channel to hold the silica bead suspension and a plastic box enclosing the assembly to prevent air currents from disturbing the assembly process. The dipcoating was conducted on an air table to reduce vibrational perturbations and the pull speed was adjusted to form uniform monolayers of beads.

Deep reactive ion etching

Silicon nanowires were formed using the silica bead layer as a mask for deep reactive ion etching using a Surface Technologies Systems Advanced Silicon Etch tool. Alternating etching (SF_6) and sidewall passivation (C_4F_8) steps using a 13.56 MHz plasma with a pulsed 380 kHz chuck bias signal allow for highly directional etching. An 8 minute etch led to 5 μm long nanowires while a 4 minute etch gave 2 μm long nanowires. The silica bead mask was removed by immersing the substrate in 10:1 H_2O:HF solution for 5 minutes.

Junction formation

The p-n junction was formed by boron diffusion using 0.1% BCl_3 in 10% H_2/Ar gas at 900 ^oC for 8 minutes. Diffusion calculations using these conditions give an expected junction depth of approximately 160 nm.

Contact formation

The back contact was made by evaporating 100 nm Ti followed by 50 nm Au immediately after a 15 s dip in 10:1 NH_4F:HF solution. The top contact was made using photolithography followed by a 30 s mild O_2 plasma and 15 s 10:1 NH_4F:HF dip and 800 nm Al followed by 200 nm Pd sputtered to form a top electrode finger pattern. The contacts were not annealed to avoid thermal mismatch-induced stress and cracking or peeling. The large-area solar cells were cut into 5 mm x 6 mm devices using an automatic wafer dicing saw.

Photovoltaic measurements

The solar cells were tested in a Janis probe station both in the dark and under simulated sunlight at 300 +/- 2 K. The solar simulator consisted of a 150 W Xe lamp, focusing optics and an AM1.5G filter from Newport. The power was tested with four different optical meters (thermopile detector type) and the average was used to set the intensity to 100 mW/cm^2. Current-voltage scans were collected at 300 mV/s. 5-10 different solar cells were tested for each combination of absorbing layer thickness and nanowire length and the reported values are the average and standard deviation of that data.

Thin silicon window formation

Double-sided polished silicon on insulator (SOI) wafers with a 7.5 μm device layer, a 500 nm buried oxide and a 525 μm handle layer were coated with about 250 nm of low-stress silicon nitride using a commercial low-pressure chemical vapor deposition system. Windows on the back-side were formed with photolithography and the silicon nitride was etched using a CF_4 plasma. The photoresist mask was removed in acetone and the silicon was etched in a 30% aqueous KOH solution at 90 ^{o}C for approximately 2.5 hours to reach the buried oxide. The end point was determined when the windows stopped bubbling. The silicon nitride mask was removed in concentrated (50%) HF. Further processing followed the procedures used on standard wafers.

Optical measurements

Transmission measurements were made with a Shimadzu NIR-UV double beam spectrometer. Equivalent apertures on both the sample and blank were used to ensure that only the window structure was in the beam path. The transmission was calibrated before each measurement and always read 100% +/-1% when there was no sample in the beam path.

Enhancement Factor (EF) calculations

1. EF from J_{sc} measurements:

The J_{sc} for solar cell 1 is given by:

$$J_{sc_1} = A_1 \cdot I_o \cdot IQE_1 \cdot q \qquad (1)$$

where A_1 is the fraction of incident light that is absorbed, I_o is the flux of incident photons per unit area, IQE_1 is the internal quantum efficiency (defined as the #electrons out/#photons absorbed) and q is the elemental charge. If we have two solar cells, 1 and 2, with the same nanowire length, diameter and spacing but with different silicon absorbing layer thicknesses, then I_o, IQE_1 and q will be the same. Therefore, if we divide J_{sc1} by J_{sc2} we get:

$$\frac{J_{sc_1}}{J_{sc_2}} = \frac{A_1}{A_2} \tag{2}$$

which demonstrates that if the charge separation and extraction efficiencies are the same, then the photocurrents are only determined by the absorption. The absorption is given by:

$$A_1 = 1 - R_1 - T_1 \tag{3}$$

where R_1 is the reflectance and T_1 is the total transmission. The total transmission is equal to the product of the three transmission components:

$$T_1 = (1 - R_1) \cdot T_{bulk_1} \cdot T_{LT_1} \tag{4}$$

where T_{bulk} is the transmission from the nanowire and bulk silicon substrate assuming standard absorption and T_{LT} is the reduced transmission due to light trapping. Substituting (3) and (4) into (2) gives:

$$\frac{J_{sc_1}}{J_{sc_2}} = \frac{(1 - R_1) \cdot (1 - T_{bulk_1} \cdot T_{LT_1})}{(1 - R_2) \cdot (1 - T_{bulk_2} \cdot T_{LT_2})} \tag{5}$$

Since the two solar cells have the same nanowire length, diameter and spacing, they should have the same reflectance and light trapping properties. With these assumptions the reflectance falls out of the expression and we can solve equation (5) for T_{LT} to give:

$$T_{LT} = \frac{J_{sc_1} - J_{sc_2}}{J_{sc_1} \cdot T_{bulk_2} - J_{sc_2} \cdot T_{bulk_1}} \tag{6}$$

T_{bulk} can be calculated with:

$$T_{bulk} = \frac{\int_{300nm}^{1100nm} e^{-\alpha(\lambda) \cdot t_{Si}} \cdot I_o(\lambda) d\lambda}{\int_{300nm}^{1100nm} I_o(\lambda) d\lambda} \tag{7}$$

where $\alpha(\lambda)$ is the absorption coefficient of silicon, $I_o(\lambda)$ is the photon flux from the AM1.5G spectrum and t_{si} is the thickness of the silicon. In order to account for the loss in absorption from the volume of silicon removed by the etching process, T_{bulk1} and T_{bulk2} have two components and are given by:

$$T_{bulk_1} = f_{NW} \cdot T_{bulk} + (1 - f_{NW}) \cdot T_{bulk-NW} \quad (8)$$

where f_{NW} is the fractional area covered by nanowires (not etched) and $T_{bulk\text{-}NW}$ is the transmission calculated for the thickness of the silicon absorbing layer in the etched areas. The effective path length for light in the silicon nanowire arrays is found by solving equation (9) for t_{LT}:

$$T_{bulk_1} \cdot T_{LT} = \frac{\int_{300nm}^{1100nm} e^{-\alpha(\lambda) \cdot t_{LT}} \cdot I_o(\lambda) d\lambda}{\int_{300nm}^{1100nm} I_o(\lambda) d\lambda} \quad (9)$$

The path length enhancement factor (EF) then is given by:

$$EF = \frac{t_{LT}}{t_{Si}} \quad (10)$$

Since there is some variation in the J_{sc} measurements, the upper bound for the EF was taken by setting J_{sc1} to the average plus the standard deviation and J_{sc2} to the average minus the standard deviation, while the lower bound used the opposite combination of averages and standard deviations.

2. EF from transmission measurements:

Figure 4 shows the transmission as a function of wavelength for thin silicon windows before and after etching. The total fraction of photons transmitted between 300 nm and 1100 nm (T_{tot}) was calculated with:

$$T_{tot} = \frac{\int_{300nm}^{1100nm} T(\lambda) \cdot I_o(\lambda) d\lambda}{\int_{300nm}^{1100nm} I_o(\lambda) d\lambda} \quad (11)$$

where $T(\lambda)$ is the measured transmission. Using T_{tot} and a reflectance of 15% for the untapered nanowire arrays (reported by Zhu et al) along with equations (4), (9) and (10) give EF values for the different nanowire arrays. Since there is some uncertainty about the amount of reduced transmission that leads to scattering versus absorption, we multiply the EF extracted from transmission measurements by a percentage that gives good agreement with the EF from the J_{sc} measurements (95% and 85% for the upper and lower bounds gives good agreement). From the data it is also apparent that the coupling percentage is related to the roughness factor; we find good agreement when we use a logarithmic relation.

Planar Transmission – Optical Model:

The transmission for a thin, double-polished, planar silicon slab can be modeled as a dielectric with two reflective surfaces (air-silicon front surface and silicon-air back

surface). This structure is called an etalon and has strong interference patterns determined by:

$$T_{etalon}(\lambda) = \frac{1}{1 + F \cdot \sin^2\left(\frac{\varphi}{2}\right)} \tag{12}$$

where F is the Finesse coefficient:

$$F = \frac{4 \cdot R}{(1-R)^2} \tag{13}$$

and $\varphi(\lambda)$ is the phase lag:

$$\varphi(\lambda) = \frac{4 \cdot \pi \cdot n \cdot t_{Si}}{\lambda} \tag{14}$$

and the reflectance is given by the Fresnel equation:

$$R = \left(\frac{n_{Si} - n_{air}}{n_{Si} + n_{air}}\right)^2 \tag{15}$$

This intensity modulation is averaged over 8 nm (slit width during measurement) and then multiplied by the transmission for the silicon slab considering a single-pass absorption:

$$T_{Si}(\lambda) = e^{-\alpha(\lambda) \cdot t_{Si}} \tag{16}$$

to give the final transmission curve.